PROCEEDINGS, 43rd Workshop on Geothermal Reservoir Engineering
Stanford University, Stanford, California, February 12-14, 2018
SGP-TR-213

Efficient simulations of heat transfer in fractured rocks

Viktoria R. Gisladottir[1], Delphine Roubinet[2] and Daniel M. Tartakovsky[3]

[1] University of California, San Diego, 9500 Gilman Drive, MC 0411, La Jolla, California, 92037 USA

[2] University of Montpellier, 34095 Montpellier Cedex 5 - France

[3] Stanford University, 367 Panama Street, Stanford, California, 94305, USA

vgislado@ucsd.edu, tartakovsky@stanford.edu

Keywords: Heat transfer, particle method, fracture network, anomalous transport, geothermal performance.

ABSTRACT

Quantitative forecasting of site-specific geothermal energy extraction requires computationally efficient simulations of heat transfer between geothermal fluids and ambient rock. Such simulations must rely on adequate representations of both heat transfer mechanisms and geological structures in which these mechanisms occur. In particular, heat transfer in fractured rocks is controlled by properties of the underlying fracture network, which can be modeled by various conceptual representations. This variety comes from the heterogeneity of fracture network properties and from challenges posed by in-situ characterization. We propose to use a mesh-free, particle-based numerical method to gain a better understanding of the impact of the fracture network properties on geothermal performance. We analyze how fracture-network topology and matrix-block size distribution control, respectively, the advective and conductive mechanisms of heat transfer in fractures and ambient matrix, as well as the heat flux exchanged between these structures. We explore two different conceptual representations of fracture networks over a range of fracture-generation parameters and hydraulic conditions.

1. INTRODUCTION

Models of heat transfer in fractured media require information about hydraulic and thermal properties of both a fluid-filled fracture network and the ambient rock matrix. Features germane to geothermal reservoirs include (i) a strong contrast between the fracture and matrix properties resulting in advective and conductive mechanisms in the fractures and matrix, respectively; (ii) topological properties of a fracture network that determine the spatial extent of a heat extraction area; and (iii) fracture-matrix heat flux exchanges that control the geothermal performances.

Fracture networks often have a hierarchical or fractal structure (Sahimi, 1993). There are many different ways to generate such networks for reservoir modeling. One example of a fractal network, commonly used to simulate solute transport in hierarchically fractured rocks, are Sierpinski lattices (Doughty and Karasaki, 2002; Roubinet et al., 2013). Another example is a Watanabe-Takahashi network (Watanabe and Takahashi, 1995), which often captures key attributes of geothermal reservoirs. Both have been successfully employed in reservoir models, where coupled fluid flow and solute/heat transport are induced by either ambient or forced hydraulic conditions. However, fractal networks with same geometrical parameters (e.g., fractal dimension) and similar physical and/or hydraulic properties can look very different from each other (Roy et al., 2007). This complicates both in-situ characterization of geothermal systems and identification of their "realistic" conceptual representations.

The presence of fractures on a large range of spatial scales and the strong contrast in properties between fractures and matrix imply that fractured reservoirs exhibit multi-scale heterogeneity. They also suggest that standard numerical models of coupled fluid flow and heat transport processes in these domains have (prohibitively) large computational cost. To tackle this challenge, we have introduced a mesh-free particle method, which was used to demonstrate the anomalous (non-Fourierian) behavior of heat transfer in fractured rocks (Gisladottir et al., 2016). Here, we use this method to simulate heat extraction in various hierarchical fracture networks at a small computational cost. Our main objectives are to compare the geothermal performances for different types of fractal networks and to analyze the impact of network properties on the computation efficiency of our method. For this purpose, we consider Sierpinski lattices and Watanabe-Takahashi networks with identical fracture density and smallest fracture length. Our analysis of the Sierpinski and Watanabe networks reveals that (i) for hydraulic regimes characterized by slow flow velocities (i.e., ambient hydraulic conditions), the geothermal performances of the two network classes differ by close to an order of magnitude, and (ii) for hydraulic regimes characterized by fast flow velocities, the differences are much smaller and the geothermal performances are of the same order of magnitude. These different behaviors are mostly due to the differences in topological properties of the Sierpinski or Watanabe networks. Additionally, the CPU efficiency is not greatly affected by the topological properties (i.e. Sierpinski vs. Watanabe), however depending on the hydraulic regime fracture density may or may not increase the computational cost. For an example of hydraulic parameters used in geothermal studies the fracture density increase did not increase computational cost.

2. PROBLEM FORMULATION

2.1 Fracture networks

Since the introduction of the notion of fractal geometry to geological structures (Mandlebrot, 1982 and Turcotte, 1992), the idea has gained support that fracture networks often have a hierarchical or fractal structure (Sahimi, 1993). Multiple fracture networks have been used for transport modeling. Sierpinski lattices are an example of synthetic fractal fracture patterns whose origin is the self-similar cataclasic model (Sammis et al., 1986). They have been used to simulate dynamic processes in hierarchically fractured rocks (Doughty and Karasaki, 2002; Roubinet et al., 2013). Watanabe and Takahashi (1995) have introduced an alternative fractal network, which captures geothermal reservoir characteristics observed in the field, using only a few parameters that can be obtained from borehole data.

In Sierpinski networks, a flow domain is subdivided into nine equal squares by two orthogonal sets of fractures. For a domain of size of L, each fracture spacing, both between the fractures and the distance from the domain border, is $L/3$. This is referred to as the template. Then N_{sq} squares are filled with the template. When the length of the template's set of orthogonal fractures is $L/3$ (and the fracture spacing is $L/3^2$), this is known as level 2. The process is then repeated until a desired level is reached. An example of a level-3 Sierpinski lattice with $N_{sq} = 3$ and orthogonal fracture set with smallest fracture length equal to $L/3^3$ is shown in **Figure 1**.

In Watanabe-Takahashi networks, the number of fractures, N_f, and the normalized length, r_i, of the ith fracture ($i = 1 \dots N_f$) are related by

$$N_f = int(C/r_0^D) \qquad r_i = C/i^{1/D} \tag{1}$$

where D is the fractal dimension, and the function $int(x)$ rounds x up to the next integer. The fracture density C and the smallest fracture length r_0 can be estimated from a core sample. The fracture aperture b is constant and the same for all fractures. A fracture network is generated by assigning each midpoint of a fracture pair a random variable. There is an equal probability that the angle between the pair of fractures takes on two prescribed values, θ_1 or θ_2.

To facilitate comparison of the Sierpinski and Watanabe networks, both are assigned the same fracture density and smallest fracture length. The former is defined as the cumulative length of fractures per area of the domain (Singhal and Gupta, 2010),

$$\rho = \sum_i r_i / L^2. \tag{2}$$

For the Sierpinski lattices the length of the smallest fracture element is used, while for the Watanabe network the smallest fracture length is r_0/L.

2.2 Fluid flow and governing equations

We consider steady-state laminar flow of an incompressible fluid in fractures embedded into impervious surrounding rock matrix. Each fracture is formed by two parallel smooth plates, resulting in the parabolic (Poiseuille) velocity profile and the average flow velocity u given by

$$u = -\left(\frac{\rho_l g b^2}{12\mu} J\right) \tag{3}$$

where ρ_l and μ are, respectively, density and dynamic viscosity of the fluid; J is the hydraulic head gradient along the fracture; and g is the gravitational acceleration constant. By applying equation (3) to each fracture segment and enforcing mass conservation at the fracture junctions, a linear system $\boldsymbol{A} = \boldsymbol{hb}$ is formed where $\boldsymbol{h}$ is the vector of the (unknown) hydraulic heads at fracture junctions (Long, 1982; Dreuzy, 2001). With a known global pressure gradient imposed on the boundaries of the domains, the linear system is solved providing the hydraulic heads necessary to compute the average flow velocity in each fracture of the network.

The particle-based method described in section 2.3, and presented in Gisladottir et al. (2016), models heat transfer in fractured media by using a solution for a single fracture embedded in an infinite matrix as a base for a probabilistic model. Heat transfer in a single fracture of aperture, b, and semi-infinite length is described by coupled boundary-value problems. One, consisting of an advection-dispersion-equation (ADE), governs temperature in the fracture, $T^f(x,z,t)$. The other, involving a diffusion equation (DE), represents temperature in the matrix, $T^m(x,z,t)$. The continuity of temperature and heat flux is enforced at the fracture-matrix interfaces, coupling these two boundary-value problems. Initially the temperature throughout the domain, both in the fracture and the matrix, is equal to T_0. The same temperature is prescribed along all external boundaries. The temperature of the injected fluid is equal to T_{inj}.

2.3 A particle-based algorithm for heat transfer

To ascertain the impact of network model selection (e.g., Sierpinski vs. Watanabe networks) and to evaluate the impact of global network properties on heat transfer, we use the mesh-free particle method presented by Gisladottir et al. (2016). For the sake of completeness we reproduce it here. The method spans three scales: i) the fracture-matrix scale where heat transfers by advection in the fractures and conduction in the infinite matrix, ii) the matrix-block scale where heat conduction is limited by neighboring fracture, and iii) the fracture-network scale where heat flux conservation is enforced at each fracture intersection and depends on the corresponding flow rate distribution.

At the fracture-matrix scale, an approximate analytical solution of the boundary-value-problems formulated in Section 2.2 takes the form (Tang et al., 1981)

$$T^f(x,t) = T_{inj} erfc\left(\frac{\varphi_m \sqrt{D_T^m} x}{2ub\sqrt{t-x/u}}\right). \quad (4)$$

It relies on the following simplifications: (i) longitudinal dispersion in the fracture is assumed to be negligible in comparison with convection, (ii) the ADE equation is averaged over the fracture aperture, and (iii) heat transfer in the matrix is assumed to be one-dimensional, perpendicular to the fracture. This analytical solution is inverted in order to evaluate the time t_{diff} spent by a "particle" in the matrix for a given displacement in the fracture. To do so, (4) is used as a probabilistic model, which replaces T^f with a uniform random generator R defined on the interval [0,1], and the result is inverted to compute corresponding random realization of t_{diff}.

At the matrix-block scale, the effects of potential neighboring fractures are taken into account by considering the case of a fracture f_i with one fracture on each side f_1 and f_2 at distance l_1 and l_2, respectively. For a particle leaving fracture f_i and diffusing into the matrix, we define P_t^1, the probability of reaching fracture f_1 without crossing fracture f_2 and P_t^2, the probability of reaching fracture f_2 without crossing fracture f_1. These first-passage-time probabilities are given analytically in the Laplace space (Feller, 1954), and back-transformed into the time domain using numerical inversion with, e.g., the Stehfest (1970) algorithm. Next, we generate P_{transfer}, the probability for a particle to transfer to one of the neighboring fractures with an associated transfer time t_{transfer} smaller than the maximum diffusion time t_{diff}, as

$$P_{\text{transfer}} = P^1_{\text{transfer}}(t_{\text{transfer}} \le t_{\text{diff}}) + P^2_{\text{transfer}}(t_{\text{transfer}} \le t_{\text{diff}}). \quad (5)$$

Once the value of P_{transfer} is evaluated, we pick a random number U from a uniform distribution on the interval [0,1]. If U is larger than P_{transfer}, the particle does not transfer to the neighboring fractures, otherwise it does and the transfer time t_{transfer} is found by solving $P_{\text{transfer}} = U$. The particle transfers to f_1 if the condition $U/U_{\max} > l_1/(l_1+l_2)$ holds with $U_{\max}=P_{\text{transfer}}$, otherwise it transfers to f_2.

At the fracture-network scale, if a particle reaches a fork intersection at the end of the fracture, the fracture to which it transfers is determined from heat flux conservation. The latter accounts for the intersection configuration and flow rate distribution as follows. The particles enter fractures with positive flow taking into account full mixing and streamline routing rules (Hull, 1986 and Berkowitz, 1994). Assuming that complete mixing takes place, the probability of a particle to enter into a fracture is the ratio of flow rate in the considered fracture to the sum of the flow rates leaving the considered intersection. If a particle can enter two fractures, the particle enters the fracture with dominant flow (LeGoc, 2009).

3. SIMULATION SET UP

In order to investigate the importance of network model selection, we consider the Sierpinski and Watanabe fracture networks embedded into a square matrix domain with side lengths of 100 m. **Figure 1** shows Sierpinski lattice networks *S1, S2,* and *S3* with N_{sq}=3 and level *M*=3, 4, and 5, respectively. The fracture densities and smallest length elements of these networks are collated in **Table 1**.

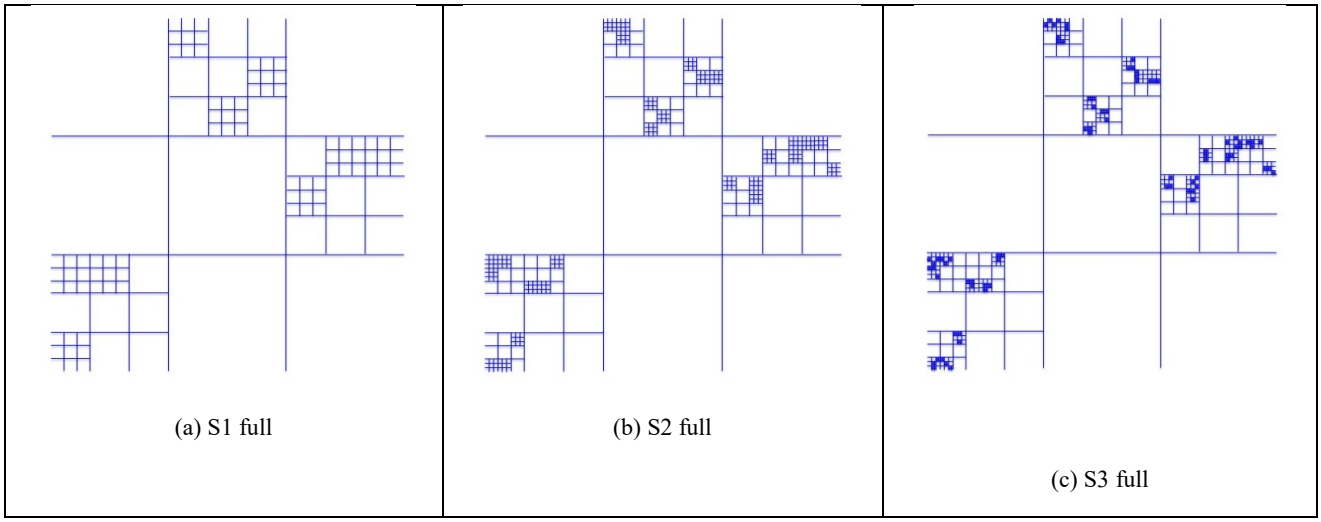

(a) S1 full (b) S2 full (c) S3 full

Figure 1. Sierpinski networks with levels M = **3 (S1, left), = 4 (S2, center), and = 5 (S3, right).**

For each of the Sierpinski networks S1, S2, and S3, there exists a Watanabe network with a similar fracture density (within 2% difference) and the same smallest fracture length (**Table 1**). Those networks are labeled Watanabe network W1, W2, and W3, respectively. They are shown in **Figure 2** with the fractures generated by equation (1) (top row) and the backbone of those fracture networks (bottom row). The Watanabe networks have the fractal dimension *D* whose values are found in the natural environment (Main, 1990; Scholz, 1993) and is employed for geothermal characteristic networks (Watanabe and Takahashi, 1995). For both networks only the fractures belonging to their respective backbones are identified based on the velocity field.

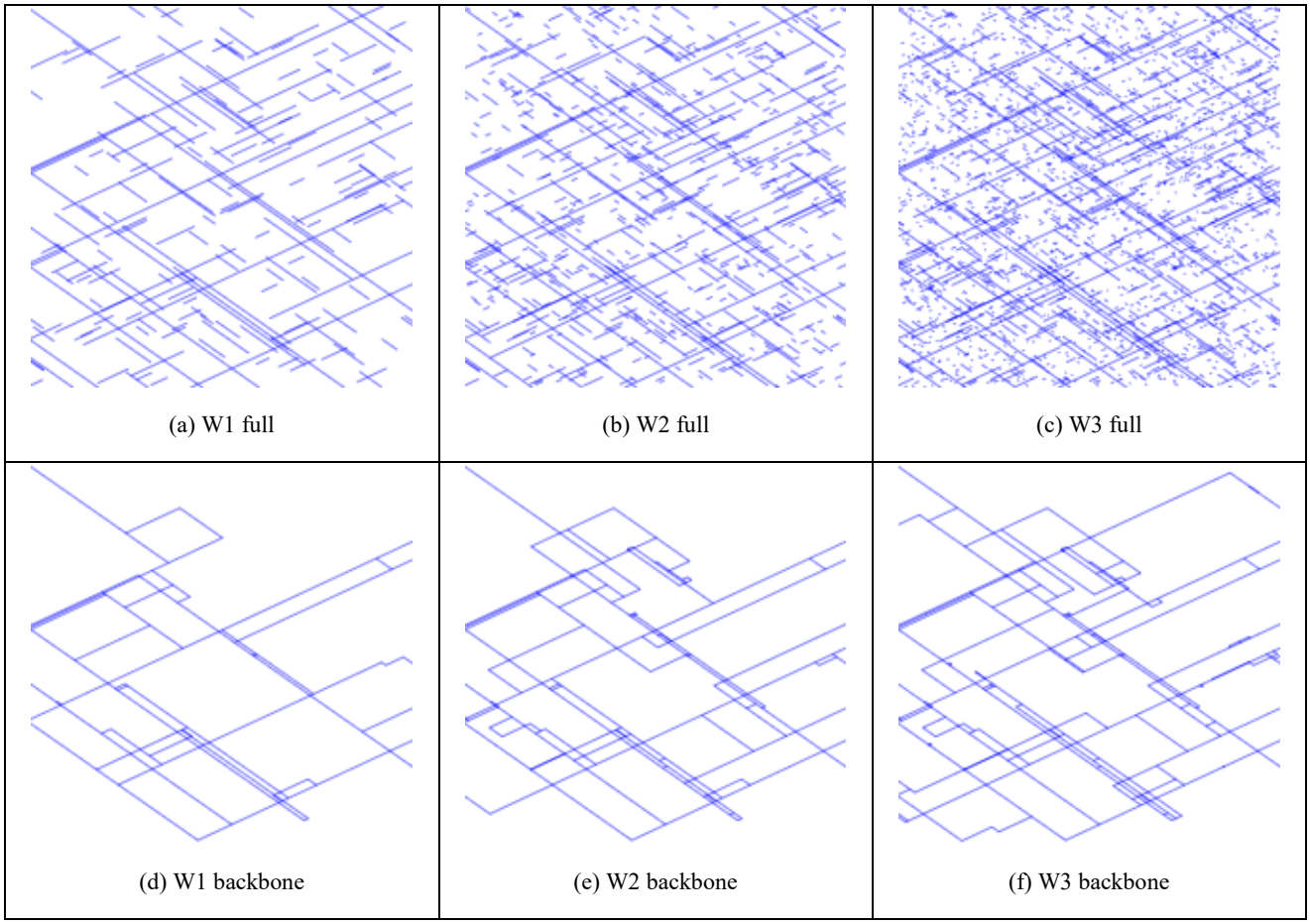

(a) W1 full (b) W2 full (c) W3 full

(d) W1 backbone (e) W2 backbone (f) W3 backbone

Figure 2. Top row: three Watanabe networks generated by equation (1) for the parameters in Table 1. Bottom row: backbones of these networks.

An injection well spans the left side of the computational domain, and the extraction well represents its right side. Fluid flow takes place from left to right through the interconnected network. To show the robustness of the prediction we look at two different hydraulic regimes between two boreholes set up for the geothermal exploitation. The first regime, called *Fast flow*, is defined with a head gradient of 1.25 and is employed in existing studies on geothermal systems (Suzuki et al., 2015). The second regime, called *Slow flow*, is defined with a head gradient set to 10^{-2} and is used for comparison. Bottom and top borders of the domain are considered to have no-flow boundaries. The flow velocity fields are generated as described in Section 2.2. with fluid density and dynamic viscosity, $\mu = 10^{-3}$ kg/(m s) and $\rho_v = 10^3$ kg/m^3, respectively. The physical properties are thermal conductivity, $k = 2.1\,\mathrm{W/(m \cdot °C)}$; rock density, $\rho_f = 2650\,\mathrm{kg/m^3}$; and rock heat capacity, $c_p = 1000\,\mathrm{J/(kg \cdot °C)}$. The Péclet number is defined as $Pe = (L * u_{\mathrm{ave}})/\alpha$ where L=100 m is the length of the domain; u_{ave} is the average flow velocity in the network (**Table 2**); and α is the thermal diffusivity $\alpha = k/(\rho_f c_p)$.

Table 1. Global parameters for Sierpinski and Watanabe networks generation.

	Fracture Density [-]	*Level M [-]*	*Frac. Density parameter, C [-]*	*Smallest fracture length [m]*
S1	0.109	3		3.7
S2	0.147	4		1.23
S3	0.185	5		0.41
W1	0.109		45	3.7
W2	0.149		22.3	1.23
W3	0.184		13.87	0.41

Reporting on geothermal reservoirs is often done in the form of $P_f = 1 - T$ where the minimum efficiency of the system is represented as $P_f = 0$ because the temperature of the extracted fluid is equal to the temperature of the (here cooler) injected fluid. Therefore the maximum efficiency of the system is represented as $P_f = 1$ corresponding to cases where the temperature of the extracted fluid is equal to the (here warmer) initial temperature of the system. **Figure 3** shows the temporal profiles $P_f(t)$ for all six networks for both hydraulic

regimes *Fast flow* and *Slow flow*. These simulations were done using $5 \cdot 10^3$ particles and they are similar to simulations performed with 10^4.

4. RESULTS AND DISCUSSION

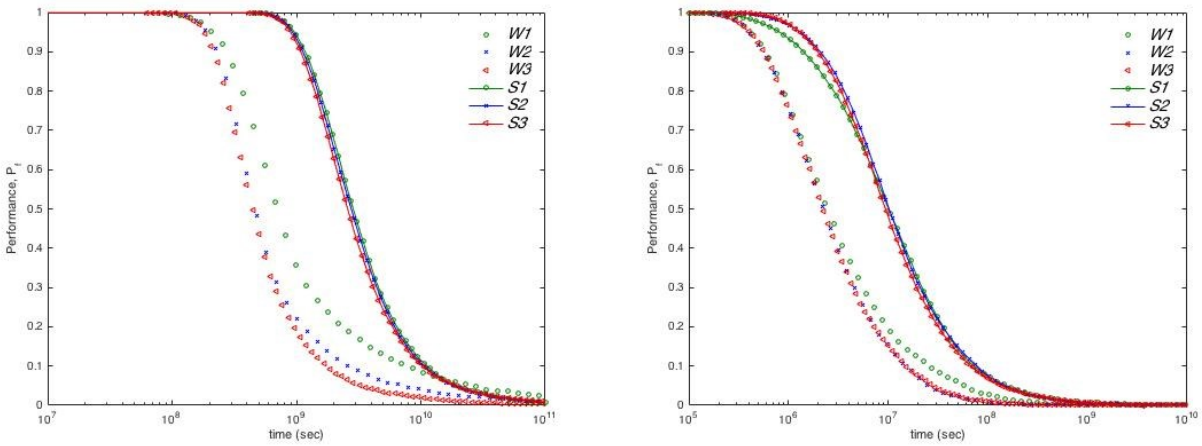

Figure 3. The Performance of the system P_f as a function of time [years] for heat transport between two boreholes 100 m apart across fracture networks: *S1, S2*, and *S3* (Figure 1) as well as *W1, W2, and W3* (Figure 2) for *Slow flow* (left) and *Fast flow* (right).

In **Figure 3** we look at the performance of the system over time at the extraction borehole on the right-hand side of the domain for all six interconnected networks *S1, S2, S3, W1, W2, and W3* presented in **Figure 1** and **Figure 2**. For *Slow* flow (left), the Watanabe networks have significantly faster drop in the performance, almost an order of magnitude, than the Sierpinski networks in which the particles appear to spend more time in the matrix. This is due to the fact that there are far more preferential pathways, fractures that span the entire domain left to right, in the Watanabe networks. When performing a simulation with the same hydraulic head on those two networks, such as here, results in higher average velocity in the Watanabe networks (due to higher number of preferential pathways) then the Sierpinski networks as is shown in **Table 2**. The increased velocity causes lower probability for the particles to enter the matrix. For both the Watanabe network and the Sierpinski network as the fracture density increases the arrival times decrease due to the limitations of the matrix block. Although there is eventually a difference between *W1* and *W2*, the performance is quite similar past the 50% drop in the performance.

Table 2. Network flow velocity values for Sierpinski and Watanabe networks for *Slow* and *Fast flow*.

Velocity [m/s]	*Slow flow Ave*	*Slow flow Min*	*Slow flow Max*	*Fast flow Ave*	*Fast flow Min*	*Fast flow Max*
S1	6.37×10^{-5}	9.57×10^{-7}	3.05×10^{-3}	7.96×10^{-2}	1.20×10^{-4}	3.81×10^{-1}
S2	3.95×10^{-4}	4.11×10^{-8}	3.12×10^{-3}	4.94×10^{-2}	5.14×10^{-6}	3.90×10^{-1}
S3	2.31×10^{-4}	6.25×10^{-10}	3.15×10^{-3}	2.89×10^{-2}	7.82×10^{-8}	3.94×10^{-1}
W1	1.18×10^{-3}	2.96×10^{-5}	3.86×10^{-3}	1.47×10^{-1}	3.70×10^{-3}	4.82×10^{-1}
W2	1.16×10^{-3}	9.46×10^{-6}	3.35×10^{-3}	1.14×10^{-1}	1.18×10^{-3}	4.19×10^{-1}
W3	1.17×10^{-3}	6.00×10^{-8}	3.47×10^{-3}	1.47×10^{-1}	7.49×10^{-6}	4.34×10^{-1}

The *Fast flow* (right) the velocity variation (**Table 2**) between the networks is not as high and hence the variance of the performance between Sierpinksi and Watanabe networks is not as stark for the *Fast flow* regime. Yet again the Watanabe networks have faster drop in the performance then the Sierpinski networks, although the difference is not as dramatic. For the Watanabe networks, initially there is not a large difference between the performances for the different fracture density networks, although the lowest fracture density network *W1*'s performance drops slightly faster to begin with. Eventually about approximately at the mean this trend reverses and the performance of *W1* drops slower than for *W2* and *W3* where the highest fracture density network *W3* has a faster drop in the performances. For Sierpinski lattices the low fracture density network *S1* starts off with faster drop in performance but also reverses roles with the high-density fracture network *S3* as time passes this happens slightly before reaching the mean. Over all the main features of the fracture network is of importance in the *Fast flow* and the matrix block only play a minor role and mostly somewhere after the mean of the performance drop. The Péclet numbers for networks *S1-S3* and *W1-W3* generated based on the average velocity presented in **Table 2** and defined in section 3 are on the $[6.95 \cdot 10^3\ 1.88 \cdot 10^5]$ range for *Slow flow* regime and the $[3.15 \cdot 10^6\ 2.35 \cdot 10^7]]$ range for *Fast flow* regime both of which are advection dominant. To begin with the all three Watanabe networks have a similar performance eventually past the 50% level of drop the *W1* performance drops slower then the other two Watanabe networks. For the Sierpinski networks initially *S1*

performance drops of faster then *S2* and *S3,* who have similar drop, but once past the 50% performance drop this reverses. Although the difference is not as much S1's performance drops slower then the other two.

To elucidate the anomalous (non Fourier like) nature of heat transfer in fracture rocks we define a relative temperature T_{inst} as the instantaneous temperature change of the injected fluid. In **Figure 4** we see the temperature distribution for the *S1, S2, S3, W1, W2, and W3* for *Fast flow* and *Slow flow* regimes. These results are obtained by taking a PDF of the original CDF distribution of the arrival times. The heavy tail found in **Figure 4** demonstrates that this anomalous behavior is found in for all of the Sierpinski and Watanabe networks in the *Fast flow* regime. Its presence is due to fracture properties as they influence fast heat propagation across the domain.

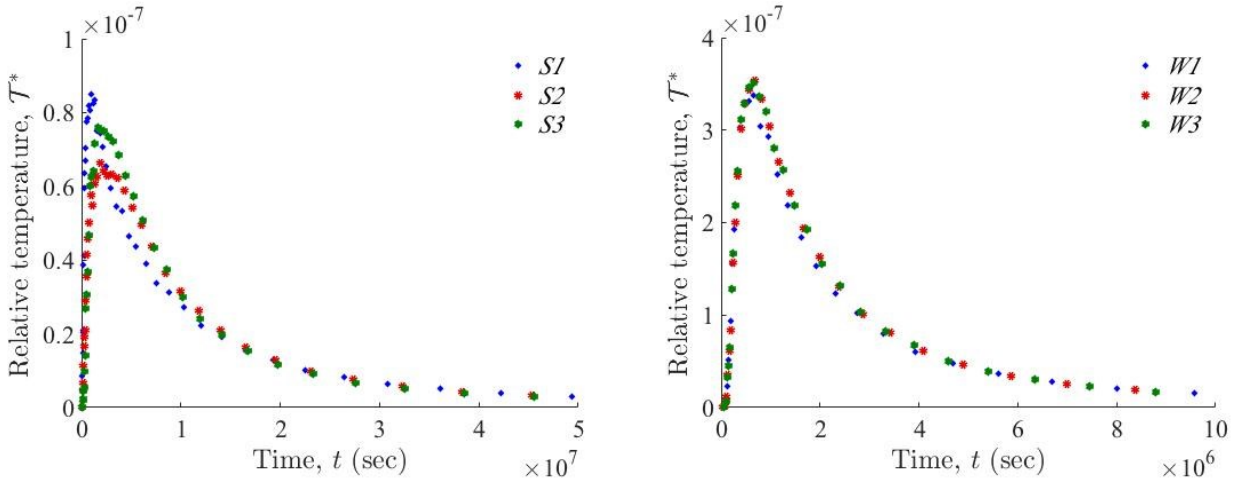

Figure 4. Temporal variability of the relative temperature of fracture networks (left) *S1, S2, S3,* (see Figure 1) and (right) *W1, W2*, and *W3* (see Figure 2) for *Fast flow* hydraulic regime.

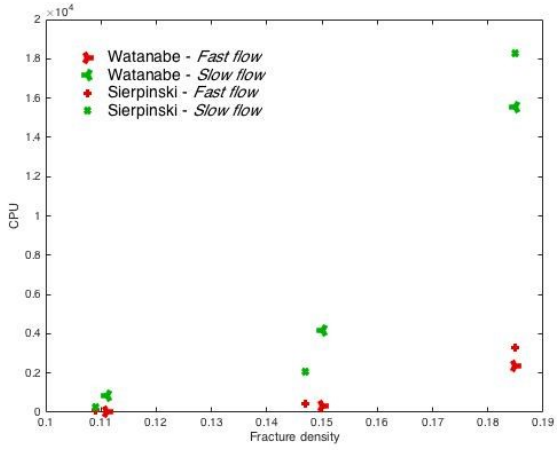

Figure 5. The CPU for the varying fracture density for the Watanabe and Sierpinski Networks for *Fast flow* and *Slow flow.*

In **Figure 5** we look at the computational cost of running the simulations of heat transport across our 100 m domain for the six networks *S1, S2, S3, W1, W2, and W3* producing the results presented in **Figure 5** as a function of their fracture density which is found in **Table 1**. For both the Sierpinski and the Watanabe networks there is significant higher CPU usage for *Slow flow* hydraulic regime for high fracture density networks. However in both case the increase is not significant for low fracture density networks. Interestingly enough for the hydraulic regime representative of those used in geothermal field studies *Fast flow* (Suzuki et al. 2015) increasing the fracture density does not increase computational cost, this applies to both Sierpinski and Watanabe networks.

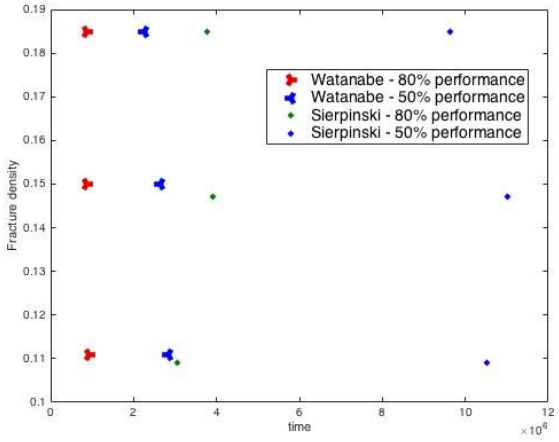

Figure 6. The temporal variation of the performance drop of the system over 100m to levels of 80% and 50% for varying degrees of fracture density for *Fast flow* hydraulic regime.

From **Figure 6** we conjure that the time it takes the performance drop of the system to level of 80% and 50% performance has more dependence on the type of fracture network then the density of the network itself. There is more significant difference on the 50% performance drop between Watanabe and Sierpinski network then for the 80%.

5. CONCLUSION

We use a computationally light mesh-free particle method to perform numerical simulations on discrete fracture networks representative of a fractured porous medium. The particle method is applied to two different networks, Sierpinski and Watanabe networks, with three sets of parameters for fracture density and smallest fracture length. For all six simulations, we have reported on performance of the system, in particular: pulse injection anomalous behavior; CPU expenditure; and levels at which we project 20% and 50% performance drops.

The results show that depending on hydraulic conditions, the propagation of a cold front across fractured domains is controlled by either the fracture network (Fast Flows) or matrix block (Slow Flows) properties. For fast flow both Sierpinski *(S2* and *S3)* and Watanabe *(W2* and *W3)* demon straight similar behaviors within in the network type although the density increases. However both of their lower density networks *S1* and *W1* very from their network type past the 50% performance drop, although *S1* additionally varies from *S2* and *S3* to begin with. There is a stark contrast between the performance drop of all three Sierpinski and all three Watanabe networks. This in turn means that the performance drop of the system to levels of 80% and 50% are far more dependent on the type of network rather then fracture density for Fast flow hydraulic regime. The heat transfer significantly deviates from the Fourier law, over a wide range of fracture densities, giving rise to anomalous effective behavior characterized by long tails. Additionally the hydraulic regime has far more impact then the topological properties as for an example of a hydraulic regime used in geothermal field studies *Fast flow* the computational cost did not significantly increase with increased fracture density.

Our results demonstrate that our algorithm takes a fraction of the time that it would take a mesh based numerical solutions of heat transfer equations. To further quantify the relative improvement we are engaged in further quantitative comparison of the particle method against a mesh method for a particular physical fracture example. Additionally, extending the studies to incorporate heterogeneity of matrix properties and for example randomly distributed fracture angles (Watanabe network) and/or heterogeneous fracture apertures (Watanabe and Sierpinski network). Our work is connected to uncertainty in site characterization (Ezzedine 2010) with Monte Carlo simulations.

We presented computationally efficient quantitative forecasting of site-specific geothermal energy extraction simulations of heat transfer between two boreholes. The hydraulic regime is the key determinant in the computational efficiency of the method and its translation into a velocity field, determined by the conceptualization of the chosen network, is to critical on geothermal performance.

6. REFERENCES

Ezzedine, S.: Impact of geological characterization uncertainties on subsurface flow using stochastic discrete fracture network models, *Proceedings,* 35th Workshop on Geothermal Reservoir Engineering, Stanford University, Stanford, CA (2010).

Feller, W.: Diffusion processes in one dimension, *Trans Am Math Soc*, **77**, (1954), 1-31.

Gisladottir, V.R., Roubinet, D., and Tartakovsky, D.M.: Particle methods for heat transfer in fractured media, *Transport in Porous Media,* **115.2**, (2016), 311-326.

Hull, L.C., and Koslow, K.N.: Streamline routing through fracture junctions, *Water Resour Res*, **12.12**, (1986), 1731–1734.

LeGoc ,R.: Caractérisation et modélisation des écoulements dans les milieu fracturés. Thèse de doctorat, Université de Rennes 1, (2009).

Long, J.C.S., Remer, J.S., Wilson, C.R., and Witherspoon, P.A.: Porous media equivalents for networks of discontinuous fractures, *Water Resour Res* **18.3**, (1982) ,645-658.

Main I.G., Meredith P.G., Sammonds P.R., and Jones C.: Influence of fractal flaw distributions on rock deformation in the brittle field, *Geol Soc London*, Special Publications, **54.1,** (1990), 81–96.

Mandelbrot, B. B.: The fractal geometry of nature. Freeman, San Francisco, (1982).

Roubinet, D., J.-R. de Dreuzy, and D. M. Tartakovsky (2013), Particle-tracking simulations of anomalous transport in hierarchically fractured rocks, *Comput. Geosci.*, **50**(SI), 52-58.

Roy, A., Perfect, E., Dunne, W.M. and McKay, L.D., Fractal characterization of fracture networks: An improved box-counting technique, *Journal of Geophysical Research: Solid Earth,* **112.B12,** (2007).

Sahimi, M.,: Flow phenomena in rocks: From continuum models to fractals, percolation, cellular automata and simulated annealing. *Reviews of Modern Physics*, **65.4**, (1993), 1393-1534.

Sammis, C.G., Osborne, R.H., Anderson, J.L., Banerdt, M., and White, P.: Self-similar cataclasis in the formation of fault gouge. *Pure and Applied Geophysics,* **124.1-2,** (1986), 53-78.

Scholz, C., Dawers, N., Yu, J.Z., Anders, M., and Cowie, P. Fault growth and fault scaling laws: preliminary results, *J Geophys Res Solid Earth*, **98.B12**, (1993), 21,951–21,961.

Singhal, B.B., Gupta, R.P.: Applied hydrogeology of fractured rocks. *Springer Science & Business Media*, (2010).

Stehfest, H.: Algorithm 368: Numerical inversion of Laplace transform. *Comm ACM,* 13.1, (1970), 47–49.

Suzuki, A., Niibori, Y., Fomin, Sa., Chugunov, Va., and Hashida, T.: Analysis of water injection in fractured reservoirs using a fractional-derivative-based mass and heat transfer model, *Math Geosci,* **47.1**, (2015), 31–49

Tang, D.H., Frind, E.O., and Sudicky, E.A.: Contaminant transport in fractured porous media: Analytical solution for a single fracture, *Water Resour Res*, **17.3**, (1981), 555–564.

Turcotte, D.L., Fractals and Chaos in Geology and Geophysics, *Cambridge University Press*, New York, (1992).

Watanabe, K. and Takahashi, H.: Fractal geometry characterization of geothermal reservoir fracture networks, *J. Geophys. Res. Solid Earth,* **100**, (1995), 521–528.